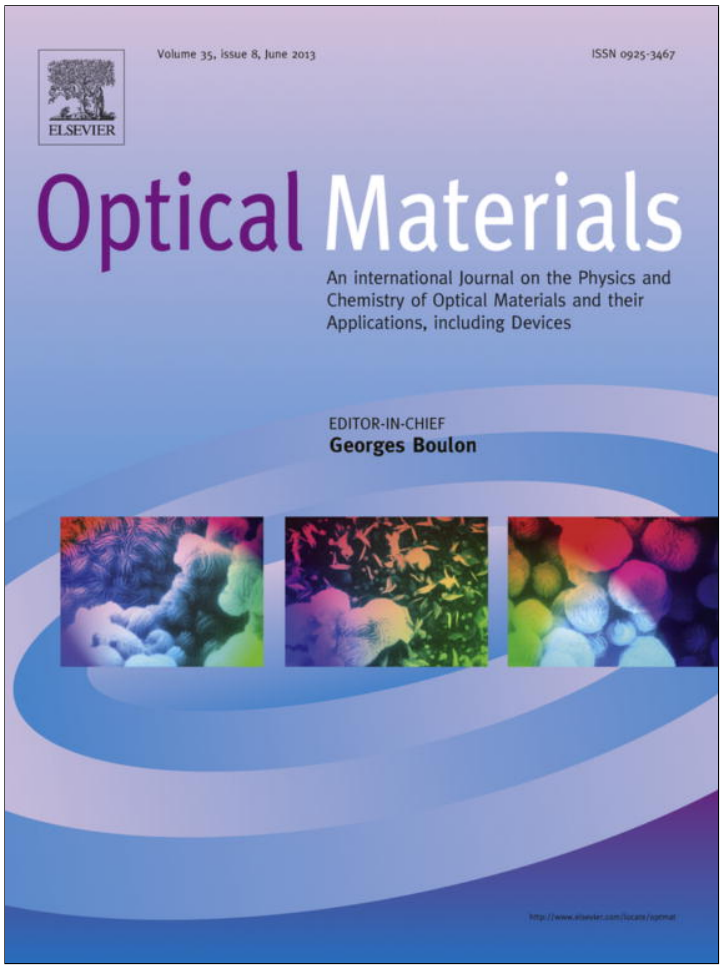

Optical Materials 35 (2013) 1595–1599

Contents lists available at SciVerse ScienceDirect

Optical Materials

journal homepage: www.elsevier.com/locate/optmat

Management of OH absorption in tellurite optical fibers and related supercontinuum generation

Inna Savelii [a], Frederic Desevedavy [a], Jean-Charles Jules [a], Gregory Gadret [a], Julien Fatome [a], Bertrand Kibler [a], Hiroyasu Kawashima [b], Yasutake Ohishi [b], Frederic Smektala [a,*]

[a] Laboratoire Interdisciplinaire Carnot de Bourgogne, UMR 6303 CNRS-Université de Bourgogne, 9 Av. A. Savary, 21078 Dijon, France
[b] Research Center for Advanced Photon Technology, Toyota Technological Institute, 2-12-1, Hisakata, Tempaku, Nagoya 468-8511, Japan

ARTICLE INFO

Article history:
Received 14 December 2012
Received in revised form 8 April 2013
Accepted 11 April 2013
Available online 11 May 2013

Keywords:
Microstructured optical fibers
Fiber losses
Nonlinear optics
Tellurite glass
Supercontinuum generation

ABSTRACT

We report the fabrication and the characterization of low OH content and low loss tellurite optical fibers. The influence of different methods of glass fabrication on fiber losses has been investigated. The use of the purest commercial raw materials can reduce the losses below 0.1 dB/m at 1.55 μm. Incorporation of fluoride ions into the tellurite glass matrix makes the optical fibers transparent up to 4 μm. A suspended core microstructured fiber has been fabricated and pumped by nanojoule-level femtosecond pulses, thus resulting in more than 2000-nm bandwidth supercontinuum after a few centimeters of propagation.

1. Introduction

The recent and intensive development of microstructured optical fibers (MOFs) [1,2] is closely related to their potential applications in various fields of research such as spectroscopy, metrology, biomedicine, imaging, telecommunications and also industrial machining and military devices [3–5]. Initial work was achieved using silica glass fibers. However, because of the multiphonon absorption of silica in the mid-IR range, studies on other glasses transparent above this wavelength range have now become of great interest in order to extend fiber functionalities beyond the current limit imposed by silica [6]. Moreover, with regard to linear and nonlinear properties of optical fibers, MOFs provide a high degree of flexibility for modeling and adjustment of fiber characteristics to suit pump source requirements [7]. Among the new candidates for non-silica MOFs, chalcogenide and tellurite glasses are especially studied for supercontinuum generation [7–11]. The $80TeO_2$–$10ZnO$–$10Na_2O$ (TZN) glass composition (mol.%) exhibits highly nonlinear properties and suitable glass stability for fiber drawing [12,13]. For these reasons, we chose to fabricate MOFs based on this glass which previously allowed us to achieve almost 1000-nm bandwidth supercontinuum pumped by a sub-nJ-level femtosecond fiber laser in the near infrared [14]. In this previous work, the spectral broadening on the long wavelength edge was limited to 2 μm due to the presence of strong OH-group absorption, which is often observed in oxide glasses [15–17]. The use of reactive chemicals and batch drying methods mentioned in Refs. [18–20] has proved to reduce the amount of water impurity incorporated into glasses. In this paper, we investigate the impact of raw materials drying and fluoride ions on the OH-group induced absorption in our fiber. We report OH-group content reduction down to almost 1 ppm and the fabrication of tellurite fibers transparent up to 4 μm. Finally we use this low OH content glass to fabricate tellurite MOFs for supercontinuum generation and we present a resulting 2160 nm spectral broadening obtained with nJ-level femtosecond pulses.

2. Experimental

2.1. Glass and MOF fabrication

We prepared tellurite glasses using pure commercial raw materials: tellurium (IV) oxide (Alfa Aesar, 99.9995%), zinc oxide (Alfa Aesar, 99.999%), and sodium carbonate (Alfa Aesar, 99.997%). In our first synthesis [14], no additional in-house purification procedures were employed to reduce moisture or eliminate trace levels of contaminants remaining in these powders. Mixed batches were melted in an open platinum crucible at 875 °C for 1.5–2 h. The syntheses under atmospheric conditions were carried out in a muffle furnace. The melt was poured into a brass mold preheated at 190 °C and subsequently annealed at the glass transition temperature (T_g) for 8 h.

* Corresponding author. Tel./fax: +33 380 39 60 29.
E-mail address: frederic.smektala@u-bourgogne.fr (F. Smektala).

0925-3467/$ - see front matter © 2013 Elsevier B.V. All rights reserved.
http://dx.doi.org/10.1016/j.optmat.2013.04.012

Atmospheric moisture and raw material contamination are evident sources for the high water content in the glass melted in ambient atmosphere. We consequently developed a fabrication process under a controlled dry atmosphere, with the help of a furnace mounted on a glove box. It must be noted that tellurite glass fabrication in a platinum crucible can involve tellurium oxide reduction [21]. Thus an oxidizing atmosphere is required and therefore the glass was synthesized in an oxygen gas flow, 4 L/min, H_2O content <0.5 ppm [17–20,22,23].

Despite the high purity of the raw materials, they contain water traces in sufficient quantity to prevent fiber transmission in the mid-IR range. That is the reason why an additional stage of raw materials batches drying should be integrated into the glass fabrication protocol [15,17,22]. Another way to remove water is the use of chemical reagents which lead to replacement of OH-groups by fluorine [18–20]. It was observed in this process that fluoride ions are incorporated into the glass matrix [19]. Note that in the case of a large amount of incorporated fluoride ions, the material properties are strongly modified towards the oxyfluoride glass family properties. As a general rule, fluoride ion incorporation into the glass matrix decreases the nonlinear material properties, but for moderate fluoride content (several mol.%) the effect is negligible and the nonlinear refractive index of fluorine containing glasses is comparable to that of fluorine free glasses [17,18].

We therefore fabricated tellurite glasses in which zinc oxide was replaced by zinc fluoride (Alfa Aesar, 99.995%) up to 50% and 100%. Each composition was fabricated in two steps, dehydration of raw materials and glass synthesis. The first dehydration step was performed in a silica tube placed inside a tubular furnace. This set up was connected to a vacuum pump and an oxygen source. The mixed batches were left under vacuum at 100 °C for approximately 18 h. They are then heated to 700 °C under oxygen gas flow at an overpressure of 100 mbar for 1–2 h, before cooling down to room temperature. After this first dehydration, the batches were introduced into a glove box in which the glass synthesis was completed under a dry atmosphere. The batches were heated to 750 °C for 2 h under oxidative conditions. During these heat treatments, Na_2CO_3 was decarbonised at 500 °C producing CO_2, and Na_2O, and for that purpose the thermal profile presents a dwell at that temperature. Ultra dry O_2 (<1 ppm H_2O) was used to reduce moisture content in atmosphere synthesis and to create an oxidizing atmosphere avoiding tellurium reduction to its metallic form which is an obstacle to light propagation. The synthesis atmosphere was both oxidizing and dry [24].

In order to improve the homogeneity of the obtained glass, a mixing operation was carried out during this synthesis step by shaking the crucible. Shaking allows removing bubbles, it also improves the glass homogeneity and allows all the melt to be in contact with the oxidizing atmosphere, thus avoiding tellurium reduction [23].

The melt was then poured into a brass mold preheated at 270 °C and subsequently annealed at approximately the glass transition temperature (T_g – 15 °C) for 8 h. The glass samples were then slowly cooled to room temperature.

Table 1 summarizes the glass fabrication process we use in this study. A typical batch weight is 55 g. The glass rod preform is typically 5 cm long for 16 mm diameter and is used for microstructured preform fabrication by a mechanical drilling. This room temperature process allows preform fabrication without any reheating of the glass after casting and provides no additional losses to final fibers [14,25,26]. Indeed, losses measured on single index fibers and losses measured on microstructured fibers are similar [26]. To drill the holes we use a drill press with drill bit of 0.8 mm in diameter and 30 mm long. We measured the roughness of the holes surface and the profile roughness parameter *Ra* was under 0.1 μm. Three 30 mm long holes of 0.8 mm diameter were drilled in a glass rod around a 1 mm diameter solid core. Then the preform was drawn into fiber under helium gas flow, in the laboratory on a commercial CIL drawing tower around 350 °C with a loading rate of 0.5 mm/min. The resulting suspended core fiber exhibited a core diameter of 2.8 μm (see Fig. 4). Standard beam propagation method simulations based on the SEM image of the fiber cross section were performed to calculate the zero dispersion wavelength that was obtained around 1.55 μm.

Table 1
Glass compositions and conditions of their fabrication.

Sample	Glass compositions (%mol)				Fabrication conditions
	TeO_2	ZnO	ZnF_2	Na_2O	
TZN–air	80	10	–	10	Room atmosphere
TZN–ox	80	10	–	10	Oxygen atmosphere
TZN-50	80	5	5	10	Oxygen atmosphere
TZN-100	80	–	10	10	Oxygen atmosphere

2.2. Thermal and optical glass properties

Differential scanning calorimetry (DSC 2920, TA Instruments) was used to determine the glass transition temperature, T_g, and the crystallization onset temperature, T_x, of the samples. The DSC curve was measured in the 20–400 °C range at a constant heating rate of 10 °C/min in N_2 atmosphere and a constant gas flux of 50 mL/min. Approximately 10–15 mg of glass bulk sample was used for measurement.

The glass rod preforms were cut into 4 mm thick slices and optically polished for spectral measurements using a Fourier Transform InfraRed spectrometer (Perkin–Elmer Spectrum One). The mid-IR absorption spectra for different thickness of samples were used for absorption coefficients in the range of 1300–6700 nm and subsequent OH-groups concentration calculations by using the following equation [19]:

$$N_{OH} = \frac{N_A}{\varepsilon \cdot L} \cdot \ln\left(\frac{1}{T}\right) \quad (1)$$

where N_A is the Avogadro constant, L the sample thickness (cm), T the transmittance and ε the molar extinction coefficient of the free OH groups in the glass. In the calculations we use the ε value of the OH groups in silicate glasses (49.1×10^3 cm^2/mol). The amount of OH present in the glass can be expressed in parts per million (ppm) [19].

2.3. Optical loss measurement

In order to estimate the OH-ion absorption influence on the fiber transparency, we measured the spectral fiber losses using an FTIR spectrophotometer (NICOLET 6700) between 1 and 5 μm as a light source for the cutback method [27]. Two single wavelength laser sources (at 1.06 μm and 1.55 μm) were also used to confirm the previous results using a 5 m long fiber sample.

2.4. Nonlinear optical properties

A Ti:Sapphire synchronously pumped optical parametric oscillator delivering 200 fs time duration pulses at a repetition rate of 76 MHz was used for measurements of the nonlinear properties. The idler output is used to pump the tellurite MOF in the anomalous dispersion regime at 1745 nm in order to generate supercontinua [26]. The pulses were injected into the MOF by means of a 20× microscope objective. The generated supercontinua are collected at the output of the fiber by a ZBLAN fiber and spectrally analyzed by two Yokogawa optical spectrum analyzers covering

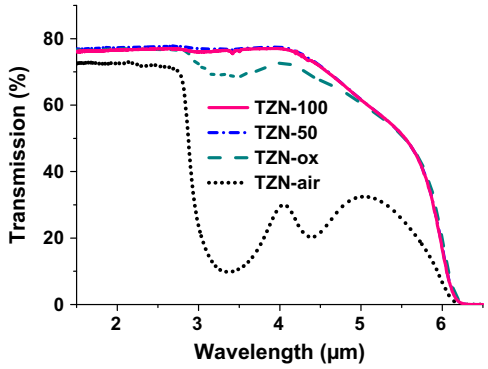

Fig. 1. TZN glasses IR transmission spectra for 4 mm thick slices.

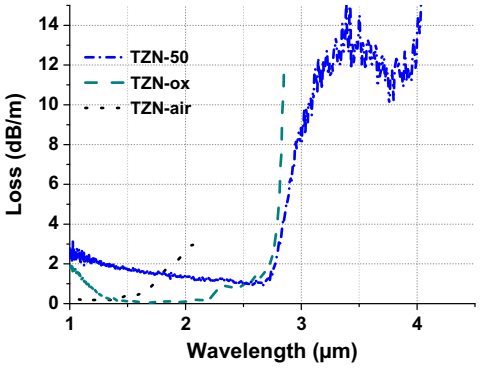

Fig. 3. Spectral losses of fabricated single index tellurite fibers.

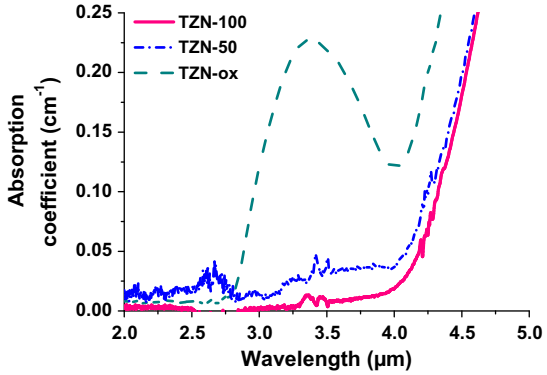

Fig. 2. TZN glasses absorption coefficients in the mid-IR range.

350–1200 nm and 1200–2400 nm, respectively, as well as an FTIR spectrometer in the range of 2.4–5 μm.

3. Results and discussion

3.1. OH-absorption in the glasses

Fig. 1 shows absorption spectra of TZN glasses fabricated in different conditions. Classically, TZN glasses exhibit absorption bands in the mid-IR range due to hydroxyl (OH) groups. A high intensity asymmetric band located around 3350 nm (2985 cm^{-1}) is identified as a combination of weakly H-bonded OH and free OH. The lower intensity band around 4350 nm (2300 cm^{-1}) is due to strongly H-bonded OH [14]. As seen in Fig. 1, the presence of OH absorption bands significantly decreases the TZN–air glass transmission for wavelengths above 3 μm. The TZN–ox glass fabricated under the dry oxygen gas flow exhibits lower absorption at 3.3 μm. In the TZN-50 and TZN-100 glasses this absorption band is strongly reduced, leading to 77% transmission from 1500 nm to 4130 nm. Fig. 2 shows the absorption coefficient curves. These data are used for subsequent OH-groups concentration calculations (Table 2).

Bonded –OH must be removed from the bulk glass, during glass synthesis, before fiber fabrication. This OH content is influenced by the free volume of the glass due to the non-bridging oxygen created by the alkaline insertion. After casting and fiber fabrication, the glass is able also to absorb free water, which can be more easily removed than the bonded one.

From these results, the glass fabrication under dry oxidizing atmosphere reduces the OH content by a factor 32. When chemical reagents containing fluoride ions are used, the OH-groups concentration is further reduced by a factor 11.5 and is estimated to be approximately 1.3 ppm in TZN-50. For TZN-100, corresponding to an oxyfluoride glass in which all ZnO has been substituted by ZnF_2, the OH-groups content is lowered to 0.5 ppm. Indeed, ZnF_2 reduce OH– content through for example the following reactions:

$$ZnF_2 + 2 - Te - OH \rightarrow ZnO + 2HF + -Te - O - Te-$$

$$ZnF_2 + H_2O \rightarrow ZnO + 2HF.$$

At the same time, it is also important to note that the glass thermal properties (Table 2) are changing as a function of the ZnF_2 ratio present within the glass. The glass transition temperature is decreased as well as the crystallization temperature. The difference between these two temperatures characterizes the glass stability. Typically, a ΔT value higher than 150 °C allows reasonable drawing possibilities. In our case, the fluoride ions incorporation decreases ΔT from 165 °C to 100–110 °C, thus complicating the fiber drawing process by favoring glass crystallization. Thus, the drawing of TZN-50 and especially TZN-100 glass preforms appears as a delicate operating process. Especially, the TZN-100 fibers are quite fragile and no further analyses were performed on them.

3.2. Low loss tellurite fibers

Before the fabrication of microstructured fibers, we first drew single index fibers from TZN–air, TZN–ox and TZN-50. Our first attempt at TZN fiber fabrication [14] led to a level of losses higher than those reported in other works, around 0.2–1.5 dB/m for the 1.3–1.6 μm region [12,13,17]. Here, using the purest commercial raw materials, we have decreased the losses to a comparable level,

Table 2
Thermal stability and OH-groups concentration for fabricated TZN glasses.

Sample	T_g (°C)	T_x (°C)	$\Delta T = T_x - T_g$ (°C)	α (10^{-3} cm^{-1})	N_{OH} (10^{18}/cm^3)	OH content (ppm)
TZN–air	285	450 [10]	165 [10]	7712	91	480
TZN–ox	285	450	165	218	2.8	15
TZN-50	265	375	110	20	0.3	1.3
TZN-100	255	360	105	8	0.1	0.5

T_g: glass transition temperature; T_x: crystallization temperature, α: absorption coefficient at 3.35 μm; N_{OH}: number of –OH groups per cm^3.

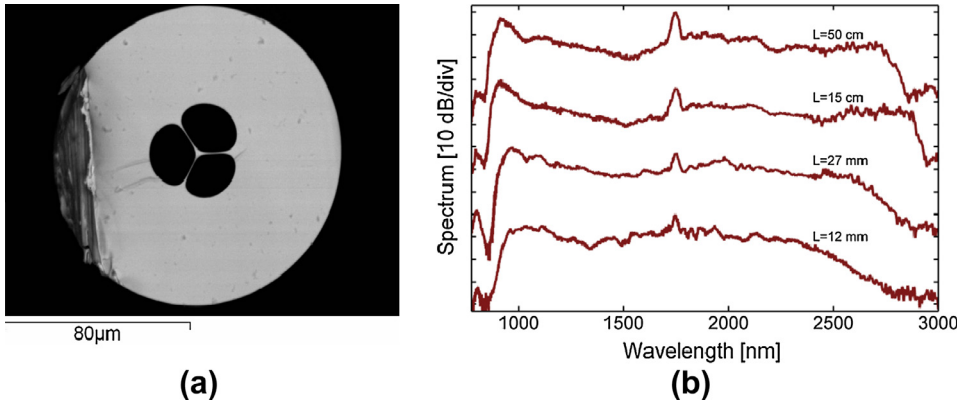

Fig. 4. (a) SEM picture of the TZN-50 MOF cross section, (b) supercontinuum generation recorded for various lengths of our TZN-50 tellurite suspended core fiber.

down to 0.4 dB/m at 1.55 µm (Fig. 3). Moreover, we have improved the fiber quality by glass fabrication under oxygen gas flow and we have succeeded in decreasing the fiber losses down to 0.1 dB/m at 1.55 µm for our single index tellurite fiber (see Fig. 3, fiber TZN–ox).

Similar results were obtained by Dorofeev [22] for tellurite fibers fabricated from ultra-pure raw materials in a purified oxygen atmosphere. In the case of TZN-50 fibers, the losses are measured to be 1.9 dB/m at 1.55 µm. This value is higher than in the case of other fibers because of glass stability reduction (Table 2) and the consequent presence of favored crystallization seeds. Note that in Wang's tellurite glasses studies [13], the level of intrinsic optical losses was theoretically estimated to be much lower, around several 10^{-3} dB/km. However, the achieved experimental level of losses is fully sufficient to perform optical experiments and characterizations. Fig. 3 presents the spectral losses of TZN single index fibers drawn in our laboratory.

3.3. OH-absorption

The TZN–air fiber fabricated under room atmosphere is not transparent for wavelengths above 2 µm because of the presence of a large amount of OH-groups. The glass fabrication under dry oxygen gas flow decreases the OH-groups concentration and allows fabrication of fiber transparent up to 3 µm. In comparison, the TZN-50 fiber shows light transmission up to 4 µm, where the multi-phonon material absorption begins [14,17,18]. The average value previously chosen (Table 2) for OH-groups extinction coefficient (49.1×10^3 cm^2/mol) leads to an estimation of 1.3 ppm of OH group for TZN-50 glass associated with 13 dB/m losses at 3.3 µm in the fiber [28]. From these results we selected the TZN-50 glass for further MOF drawing. Due to the small core of the MOFs the spectral loss measurements are not possible using our set-up. However, in previous work [14,26] we have shown that the optical losses in the single index fibers and in the MOF are similar.

3.4. Supercontinuum generation

In order to investigate nonlinear propagation in our low-loss tellurite fibers we use a TZN-50 suspended-core MOF pumped by the 200-fs femtosecond laser in its anomalous dispersion regime at 1745 nm. A spectral broadening over 2000 nm can be achieved in various fiber lengths (see Fig. 4) and for maximum input pulse energy about 1.3 nJ. The almost two octaves supercontinuum (SC) generation extends in the infrared from 840 nm to 3000 nm. Above 3000 nm, the effects of OH-absorption are clearly observed when fiber length exceeds 15 cm, thus preventing the further spectral broadening towards longer wavelengths for the 50 cm long segment. The SC generation obtained is considerably improved compared to our first attempts [14]. However, despite a strong reduction of hydroxyl group pollution in the glass and a great improvement of its optical quality, the supercontinuum extension obtained in the TZN MOFs is similar to that obtained in our previous work [26] in which the OH level corresponding to TZN–ox glasses was around 15 ppm. Thus, for the moment we are still limited around 3 µm in SC extension for such nJ-level pumping and fiber length. From numerical simulations the low remaining OH-groups (~1 ppm) in our tellurite glass is however expected to allow SC generation further in the mid-infrared range. We will reconsider the observed limitation around 3 µm in future works.

4. Conclusion

In summary, we report that the use of the purest commercial raw materials combined with the incorporation of fluoride ions into a tellurite glass matrix enables the fabrication of tellurite-based optical fibers transparent up to 4 µm with a minimum of losses of 0.1 dB/m at 1.55 µm, and an OH level reduced to around 1 ppm. A suspended core fiber (2.8-µm core diameter) based on this low OH content glass has then been drawn and has been successfully pumped by nJ-level femtosecond pulses, thus resulting in more than 2000-nm bandwidth supercontinuum still limited beyond 3 µm. Further work will be devoted to exceeding this limitation to reach supercontinuum generation in the whole range between 1 and at least 4 µm.

Acknowledgments

This work was supported by the Regional Council of Burgundy, the French National Research Agency through the Confian project and the PHC Egide program Sakura. It has been performed in cooperation with the Labex ACTION Program (Contract ANR-11-LABX-01-01).

References

[1] P.St.J. Russell, IEEE J. Lightwave Technol. 24 (2006) 4729–4749.
[2] J. Laegsgaard, A. Bjarklev, J. Am. Ceram. Soc. 89 (2006) 2–12.
[3] R. Holzwarth, T. Udem, T.W. Hänsch, J.C. Knight, W.J. Wadsworth, P.St.J. Russell, Phys. Rev. Lett. 85 (2000) 2264–2267.
[4] I. Hartl, X.D. Li, C. Chudoba, R.K. Ghanta, T.H. Ko, J.G. Fujimoto, J.K. Ranka, R.S. Windeler, Opt. Lett. 26 (2001) 608–610.
[5] J. Price, W. Belardi, T. Monro, A. Malinowski, A. Piper, D. Richardson, Opt. Exp. 10 (2002) 382–387.
[6] J.H.V. Price, T.M. Monro, H. Ebendorff-Heidepriem, F. Poletti, P. Horak, V. Finazzi, J.Y.Y. Leong, P. Petropoulos, J.C. Flanagan, G. Brambilla, X. Feng, D.J. Richardson, IEEE J. Sel. Top. Quantum Electron. 13 (2007) 738–749.

[7] X. Feng, W.H. Loh, J.C. Flanagan, A. Camerlingo, S. Dasgupta, P. Petropoulos, P. Horak, K.E. Frampton, N.M. White, J.H.V. Price, H.N. Rutt, D.J. Richardson, Opt. Express 16 (2008) 13651–13656.
[8] J. Fatome, B. Kibler, M. El-Amraoui, J.C. Jules, G. Gadret, D. Desevedavy, F. Smektala, Electron. Lett. 47 (2011) 398–400.
[9] D.D. Hudson, S.A. Dekker, E.C. Mägi, A.C. Judge, S.D. Jackson, E. Li, J.S. Sanghera, L.B. Shaw, I.D. Aggarwal, B.J. Eggleton, Opt. Lett. 36 (2011) 1122–1124.
[10] P. Domachuk, N.A. Wolchover, M. Cronin-Golomb, A. Wang, A.K. George, C.M.B. Cordeiro, J.C. Knight, F.G. Omenetto, Opt. Express 16 (2008) 7161–7168.
[11] M. Liao, X. Yan, G. Qin, C. Chaudhari, T. Suzuki, Y. Ohishi, Opt. Express 17 (2009) 15481–15490.
[12] E. Snitzer, E.M. Vogel, J.S. Wang, U.S. Patent (1993) 5251062.
[13] J.S. Wang, E.M. Vogel, E. Snitzer, Opt. Mater. 3 (1994) 187–203.
[14] I. Savelii, J.C. Jules, G. Gadret, B. Kibler, J. Fatome, M. El-Amraoui, N. Manikandan, X. Zheng, F. Désévédavy, J.M. Dudley, J. Troles, L. Brilland, G. Renversez, F. Smektala, Opt. Mater. 33 (2011) 1661–1666.
[15] M.F. Churbanov, A.N. Moiseev, A.V. Chilyasov, V.V. Dorofeev, I.A. Kraev, M.M. Lipatova, T.V. Kotereva, E.M. Dianov, V.G. Plotnichenko, E.B. Kryukova, J. Optoelectron. Adv. Mater. 9 (2007) 3229–3234.
[16] A.M. Efimov, V.G. Pogareva, J. Non-Cryst. Solids 275 (2000) 189–198.
[17] A. Lin, A. Zhang, E.J. Bushong, J. Toulouse, Opt. Express 17 (2009) 16716–16721.
[18] A. Lin, A. Ryasnyanskiy, J. Toulouse, Opt. Lett. 36 (2011) 740–742.
[19] J. Massera, A. Haldeman, J. Jackson, C. Rivero-Baleine, L. Petit, K. Richardson, J. Am. Ceram. Soc. 94 (2011) 130–136.
[20] M.D. O'Donnell, C.A. Miller, D. Furniss, V.K. Tikhomirov, A.B. Seddon, J. Non-Cryst. Solids 331 (2003) 48–57.
[21] I. Savelii, J.C. Jules, G. Gadret, B. Kibler, J. Fatome, M. El-Amraoui, F. Désévédavy, J.M. Dudley, J. Troles, L. Brilland, G. Renversez, F. Smektala, Proc. SPIE 8073 (2011) 80732G.
[22] V.V. Dorofeev, A.N. Moiseev, M.F. Churbanov, T.V. Kotereva, A.V. Chilyasov, I.A. Kraev, V.G. Pimenov, L.A. Ketkova, E.M. Dianov, V.G. Plotnichenko, A.F. Kosolapov, V.V. Koltashev, J. Non-Cryst. Solids 357 (2011) 2366–2370.
[23] H. Ebendorff-Heidepriem, K. Kuan, M.R. Oermann, K. Knight, T.M. Monro, Opt. Mater. Express 2 (2012) 432–442.
[24] J. Massera, A. Haldeman, J. Jackson, C. Rivero-Baleine, L. Petit, K. Richardson, J. Am. Ceram. Soc. 94 (1) (2011) 130–136.
[25] L. Brilland, J. Troles, P. Houizot, F. Desevedavy, Q. Coulombier, G. Renversez, T. Chartier, T.N. Nguyen, J.L. Adam, N. Traynor, J. Ceram. Soc. Jpn. 116 (2008) 1024–1027.
[26] I. Savelli, O. Mousawad, J. Fatome, B. Kibler, F. Desevedavy, G. Gadret, J.C. Jules, P.Y. Bony, H. Kawashima, W. Gao, T. Kohoutek, T. Suzuki, Y. Ohishi, F. Smektala, Opt. Express 20 (2012) 27083–27096.
[27] I.P. Kaminow, L.W. Stulz, Appl. Phys. Lett. 33 (1978) 62.
[28] O. Humbach, H. Fabian, U. Grzesik, U. Haken, W. Heitmann, J. Non-Cryst. Solids 203 (1996) 19–26.